WAVEFORM CLASSIFICATION AND RETRACKING OF JASON-2 AND JASON-3 IN HALMAHERA SEA

Maya Eria Sinurat[a*], Bisman Nababan[b], Jonson Lumban Gaol[b], Henry Munandar Manik[a], Nurul Hazrina Idris[c,d]

[a]Marine Technology Graduate Study Program, Faculty of Fisheries & Marine Science, IPB University, Bogor, Indonesia
[b]Department of Marine Science and Technology, Faculty of Fisheries & Marine Science, IPB University, Bogor, Indonesia
[c]Tropical Resource Mapping Research Group, Department of Geoinformation, Faculty of Built Environment and Surveying, Universiti Teknologi Malaysia, 81310 UTM Johor Bahru, Johor Malaysia
[d]Geoscience and Digital Earth Centre, Research Institute for Sustainability and Environment, Universiti Teknologi Malaysia, 81310 UTM Johor Bahru, Johor Malaysia

Graphical abstract
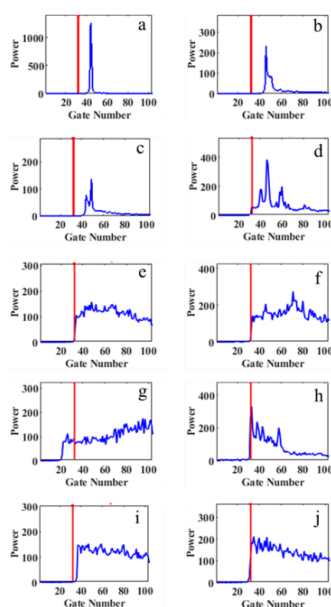
Abstract

The accuracy of sea surface heights (SSHs) estimation from satellite altimeters is strongly influenced by the microwave reflected signals (or waveforms). Waveforms in open oceans generally have ideal shapes following the Brown (1977) model. However, in coastal and shallow waters, the signals are disturbed by lands, thus resulting in complicated waveforms (non-Brown). Non-Brown waveforms produce inaccurate SSH estimations; therefore, specialized protocols such as waveform classification and retracking are crucial when attempting to produce accurate estimations. In this study, waveforms of Jason-2 and Jason-3 satellite altimeters in the Halmahera were classified and retracked using several algorithms, such as Offset Centre of Gravity (OCOG), Ice, Threshold, and Improved Threshold. The results showed that waveforms in the Halmahera Sea had ten generic classes with dominant class of the Browns. The validation results showed that all retrackers (except OCOG) had the value of correlations exceeding 0.75, and Root Mean Square Error (RMSE) smaller than 25 cm at a distance of 5-20 km from the land. The Threshold 10% was the most common retracker that appeared with the highest improvement percentage (IMP), meanwhile the Ice retracker consistently produced the best correlation (0.86) and the lowest RMSE (16cm). The retracking results showed that waveform retracking generally can improve SSH estimation accuracy from ocean (standard) retracker.

Keywords: Coastal altimetry, classification, retracking, Jason-2, Jason-3

1.0 INTRODUCTION

Indonesia is an archipelagic country, which contains of 17,504 islands and has long coastline of 99,093 km.

Indonesia also has high variability of sea levels, thus making it vulnerable to sea level rise. The sea level rise in Indonesia is about 4.2 – 5.8 mm/year or higher up to twofold of the world sea level rise rate [1, 2, 3]. The

extreme sea level rise has negative impacts on the coastal environments and small islands, such as the possibility of flooding and inundation for coastal areas. Therefore, it is important to monitor the spatial and temporal dynamics of sea level there accurately.

Many satellite altimeters have been launched into space to measure sea surface heights (SSHs) that can support many oceanographic studies [4]. In terms of spatial and temporal coverages, satellite altimeters can provide more SSHs data than tide gauge measurements. Jason series is a satellite altimetry mission that has high temporal resolution (~10 day). The Jason-2 (launched in 2008) and Jason-3 (launched in 2016) altimetric missions are capable of producing accurate SSHs estimations with high accuracy of up to 2.5 cm in the open ocean [5, 6].

In many cases, the accuracy of altimetric SSHs is influenced by the shape of waveforms. Waveform is a function of time and the power signals reflected from the earth's surface [7, 8]. In general, waveforms over homogeneous surface such as the open ocean have the ideal shape that can be described by the Brown model [9]. The Brown waveform has three main parts: thermal noise; leading edge; and trailing edge [8, 10]. Thermal noise has flat pattern and is the part when the time signals have not reached the sea surface. The leading edge is the part when the signals hit the sea surface (nadir), thus resulting in the ramp pattern with increasing power. The trailing edge is a reflection of wave energy around the nadir [8].

SSHs estimation can be obtained by measuring the distance of satellites to the surface of the earth (or range) at the midpoint of the leading edge (or tracking point) [11]. However, in coastal waters, the waveform is contaminated by reflections on the land topography and the condition of the surrounding waters causing the waveform pattern to become complex (non-Brown waveform). This affects the leading edge position, which might shift depending on the water's condition, thus leading to a false SSHs estimation [10, 11, 12, 13, 14, 15, 16].

One of standard protocols to improve the accuracy of SSHs in coastal areas is waveform retracking [10, 11, 12, 14, 17]. This is a ground processing technique to re-calculate the altimetric geophysical parameters, particularly the SSHs, by fitting and/or applying the waveforms to the appropriate retrackers [11]. Many studies have succeeded in increasing the accuracy of SSHs estimation in coastal areas with waveform retracking e.g., [11, 12, 16, 17, 18, 19, 20, 21]. [12] succeeded in increasing the accuracy of Geosat altimeter data waveform in Taiwan waters up to 20%. [15] retracked the Envisat waveforms in the Mediterranean sea with the highest improvement percentage of 59.8%. In 2012, [19] increased the accuracy of Jason-1 and Jason-2 data in Australia around the Great Barrier Reef up to 86.96% with waveform retracking.

Although various studies have been conducted to evaluate the performance of waveform retracking worldwide, their performance varies depending on water conditions and coastal topographies [15, 22].

Therefore, it was necessary to identify waveform types, retrack waveforms, and validate the waveform retracking results with local tide gauge data.

Across Southeast Asia, several studies have been conducted to assess the retracking performance over the marginal seas [11, 20, 23, 24, 25, 26, 27, 28, 29]. The performance can be determined by comparing with geoidal height data and tide gauge data.

Over the Indonesian seas, previous studies (e.g., [23, 25, 28, 29]) reported the performance of several retrackers using the geoidal height data, which highlighting the precision of retracked SSHs. While the accuracy of the retrackers is also valuable, such studies are yet to be done, thus becoming the motivation of this study.

In this study, the regional performance of Jason-2 and Jason-3 altimetric data over the complicated oceans at Halmahera Sea, Indonesia were assessed. This included the analysis of waveform classes, waveform retracking, and local accuracy assessment by comparing the retracking results with both geoid and tide gauge data. The focus of waveform classification in this study was to determine the changes in water conditions (i.e. distance from coastal areas and water depth) on the shape of the altimetry signal. The waveform classification was then useful for statistically describing the predominance of waveform shape in a particular area [8]. This study also intended to find the reliability of altimetric data, both without and with waveform retracking, over the complicated experimental regions, thus enabling operational studies such as sea level rise and coastal management.

2.0 STUDY SITE AND DATA

The study site was over Halmahera Sea, Indonesia at 127°24'59.38"E-130°24'40.22"E and 2°29'35.84"N-1°57'24.89"S (Figure 1). The Halmahera Sea has complex topography with varying depths from shallow (depth <200 m) to deep sea (depth >200 m). It is directly related to the Pacific Ocean, and crossed by the Indonesian throughflow. The existence of several bays and small islands in the Halmahera Sea further adds to the complexity of the water dynamics, which affect the signal reflections received by the satellite altimeter.

This study utilized the satellite altimetry data from sensor geophysical data record (SGDR) type-D of Jason-2 (passes 75 and 164) from October 2016 to June 2017, and of Jason-3 (passes 164 and 253) from September 2016 to December 2018. They were high resolution (20Hz) data comprising of waveforms with 1-104 gates.

Bathymetry data were obtained from the National Bathymetry (BATNAS) published by National Geospatial and Information Agency of Indonesia (BIG) with a resolution of 6". The bathymetry data were used in the analysis of waveform classes.

For validation purpose, data from geoid model and tide gauge were used. The geoid data were based on the global geoid undulation model of Earth Gravitational Model 2008 (EGM08). It referred to the Geodetic System 1984 (WGS84) as the description of the earth's surface topography. The hourly tide gauge data were acquired from the Gebe port (TG Gebe) station recorded by BIG located about 30 km from track 164 of Jason-3.
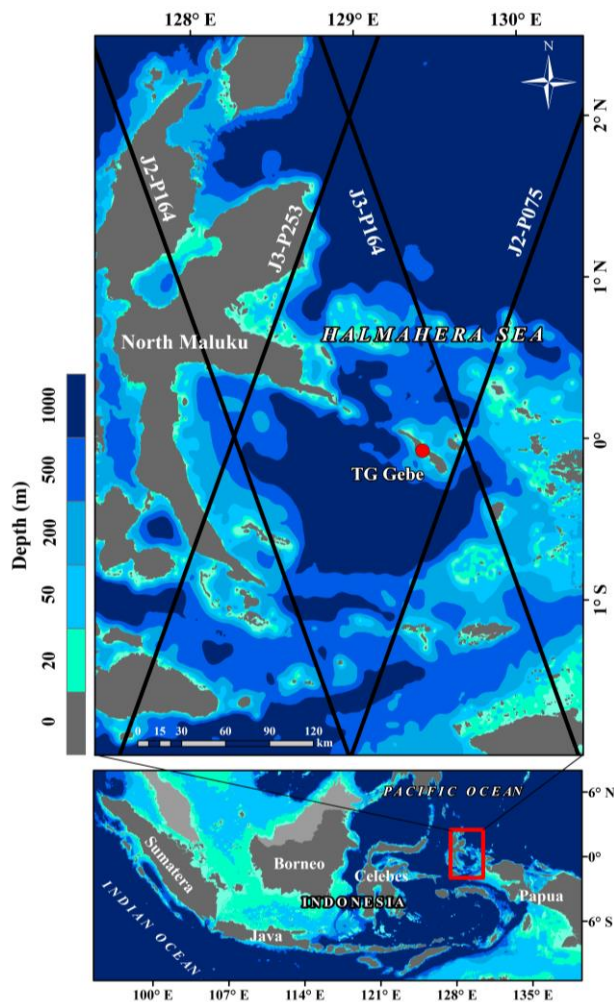
Figure 1 The study site over Halmahera Sea. Grey color is the land and shaded blue colors are sea depths. The black lines indicate tracks from Jason-2 (J2) and Jason-3 (J3). The location of Gebe tide gauge station is shown in red point

3.0 METHODOLOGY

3.1 Waveform Classification

The Jason-2 and Jason-3 waveforms were classified using Support Vector Machine (SVM), a supervised learning machine technique that had a non-parametric algorithm and was based on statistical learning theory. The objective of the SVM algorithm was to find the location of decision boundaries that produce the optimal grouping of classes. SVM built an optimal hyperplane as a decision surface based on the greatest margin between the classes [30].

Classification using SVM involved two important steps: 1) the training mode using selective waveform samples; and 2) the simulating mode in which the trained SVM was applied to the remaining waveforms. According to [31], sufficient amount of training data are needed when training the SVM. It was stated that 70 training data in each class might produce accurate classification results; however, larger size of training data can provide more accurate results. In the training mode, the SVM was fed with samples from waveform. It consisted of 1,000 samples comprising of 500 Brown waveforms and 500 non-Brown waveforms. The training mode generated a model from SVM algorithm that contained optimized parameters. In the simulating mode, the classes of the remaining waveforms were predicted based on the trained model.

In this study, SVM were used to classify waveforms into two main classes, Brown and non-Brown. The dominant waveform classes in Halmahera were then identified visually (or manually). Identification of dominant classes was conducted by grouping waveforms based on the shape and positon of the leading edge. The shapes were categorized based on the modification of the waveform shape classes made by [8]. The classes were then analyzed by water depth and distance from the coast.

3.2 Waveform Retracking

In attempting to produce accurate SSHs, several retracking algorithms were performed. They were based on the freely available Ocean (or Maximum Likelihood Estimator-4, MLE4)[32] and Ice [33] retrackers from SGDR-D data, and the retrackers of Offset Center of Gravity (OCOG) [34], Threshold [35,36], and Improved Threshold [12]. The Threshold and Improved Threshold algorithms were implement-ted with threshold values of 10%, 20%, and 50%. Detailed descriptions about the retracking algorithms were available from [12, 32, 33, 34, 35, 36].

Retracking with several algorithms optimized the mid-point gate of the leading edge (related to the range and SSHs). This can be applied in Eq.1 to correct the midpoint gate estimated by the on-board tracker [15, 37, 38]:

$$d_r = \frac{c \times \Delta G_a}{2} \times (G_r - G_0) \qquad (1)$$

where, d_r is the retracked range correction (m), c is the speed of light (299792458 m/s), ΔG_a is the time interval for one gate, G_r is the gate number of midpoint leading edge resulted from retracking (i.e. Ice, OCOG, Threshold, and Improved Threshold), and G_0 is the nominal tracking gate (31 for J2 and J3).

The retracked range (R_r) were obtained by adding the on-board tracker range (R) with the range correction (dr).

$$R_r = R + d_r \tag{2}$$

The SSH estimation resulting from retracking can be calculated using the following equation [13, 39]):

$$SSH = H - R_r - \Delta h_{dry} - \Delta h_{wet} - \Delta h_{iono} - \Delta h_{ssb} - h_{tides} - h_{atm} \tag{3}$$

where, H is satellite altitude and h corrections are sea surface height corrections (e.g., $\Delta h_{dry} = -\Delta h_{dry}$). In producing accurate SSH, the range should be corrected from the atmosphere and ocean geophysical effects. This includes the dry tropospheric correction (Δh_{dry}) and inverted barometric height correction combined with high-frequency fluctuations (h_{atm}) from the European Centre for Medium-Range Weather Forecasts (ECMWF), the wet tropospheric correction (Δh_{wet}) from the advanced microwave radiometric (AMR) detector, ionospheric correction (Δh_{iono}) from the Poseidon-3B on Jason satellite, and sea state bias correction (Δh_{ssb}) based on empirical solution on GDR data [40].

The oceanographic signals, such as tidal signals, also need to correct in order to avoid significant aliasing errors. There are several tide corrections (h_{tides}) need to be removed i.e., pole tide, solid earth tide and geocentric tide. In this study, the pole tide and solid tide used were from GDR data, while the geocentric tide was corrected by using the harmonic analysis from t-tide technique [41].

3.3 Accuracy Assessment

The quality of altimetric data was assessed by comparing with quasi-independent geoid height data and tide gauge. Comparison with geoid heights was intended to finding the data precision, meanwhile comparison with tide gauge was aimed to find both the precision and accuracy.

3.3.1 Comparison with Geoid Data

The performance of the waveform retracking against geoid data was calculating using the Improvement Percentage (IMP). From there, the best retracker can be identified. The IMP of several retracking algorithms were calculated by finding the standard deviation (SD) of the difference between SSHs and geoid [12,38] using the following equations:

$$\sigma_{Ocean \, (or \, Retracking)} = \left(\frac{1}{N}\sum_{i=1}^{N}(x_i - \bar{x})^2\right)^{\frac{1}{2}} \tag{5}$$

$$IMP = \frac{\sigma_{Ocean} - \sigma_{Retracking}}{\sigma_{Ocean}} \times 100\% \tag{6}$$

where, σ_{Ocean} is the SD of the difference between the SSHs from ocean retracker and geoid height, and $\sigma_{Retracking}$ is the SD of the difference between the SSHs from the retracking and geoid height. x_i is value of the ith point in SSHs data set (from respective retracker), $\bar{x}$ is the mean value of SSH data set, and N is the number of data points in the SSHs data set.

3.3.2 Comparison/Validation with Tide Gauge

For validation, the sea level anomalies (SLAs) resulting from waveform retracking were compared to the tide gauge data. The retracked SLAs were obtained by subtracting SSHs from mean sea surface (MSS). MSS data were based on MSS_CNES-CLS11 model provided in SGDR-D data. SLAs was calculated using the following equation:

$$SLA = SSH - MSS \tag{7}$$

To ensure consistency between altimetric retracked SLAs and tide gauge, the mean value of SLA time series from tide gauge was computed, and subsequently subtracted from the tide gauge SLAs to obtain the anomaly. Then, the t-tide technique [41] was applied to produce non-tidal SLAs from tide gauge. This technique was applied to get better tidal signals model [42], particularly for coastal oceans with varying geophysical processes [43].

Concerning the temporal differences between both datasets (i.e., altimetry is every 9.999 days, and tide gauge is an hourly data), the hourly tide gauge data was searched at the closest time as the altimetry data. This is to enable comparison between them.

The retracked SLAs were statistically analyzed by computing the correlation (r) and root-mean-square error (RMSE) using the following equation [44]:

$$r = \frac{c_{x,y}^2}{(S_x S_y)} \tag{8}$$

$$RMSE = \left(\frac{1}{N}\sum_{i=1}^{N}(x_i - y_i)^2\right)^{\frac{1}{2}} \tag{9}$$

where, x is the SLAs resulting from waveform retracking, y is the tide gauge data, $c_{x,y}^2$ is co-variant, S_x and S_y are the standard deviations and N is the number of data.

4.0 RESULTS AND DISCUSSIONS

This section described the results of waveform classification (Section 4.1) and the waveform retracking (Section 4.2 and 4.3). In Section 4.1, the percentage of waveform classes were computed and the dominant waveform classes were performed. In Section 4.2 and Section 4.3, the retracked SSHs and SLAs were evaluated using geoid height and tide gauge, respectively.

4.1 Waveform Classes in Halmahera Sea

The SVM classifier produced two classes of waveforms: 1) Brown; and 2) non-Brown. Table 1 summarizes the findings by showing the percentage of waveform classes for the four satellite tracks. In general, the mean percentage of Brown class was larger (56%) to that of the non-Brown class (44%). However, it seemed

that the percentage of Brown class over the study site was extremely lower when compared to other study regions in Southeast Asia. For example, the percentage of Brown waveforms >90% [24] over the South China Sea, ~94% [25] over Java Sea, and 95% [29] over Natuna Sea. Furthermore, [45] found 91% non-ocean like waveforms of Sentinel-3A Synthetic Aperture Radar (SAR) altimetry over the marginal seas at Southeast Asia.

Table 1 Mean percentage of Brown and non-Brown waveforms in the Halmahera Sea. The number of cycles are indicated as superscript letters a, b, c, and d

Track	Number of waveforms	Percentage (%)	
		Brown	*non-Brown*
J2-P075[a]	31822	75	25
J2-P164[b]	25905	60	40
J3-P164[c]	142834	49	51
J3-P253[d]	122683	40	60
Mean		56	44

[a]20 cycles, [b]21 cycles, [c]85 cycles, [d]84 cycles

The percentage of Jason-2 Brown class (>60%) was found superior to that of non-Brown class (<40%). Opposite findings were reported for Jason-3, in which the percentage of non-Brown (>51%) was always higher to that the Brown class (<50%). It was also seen that the percentage of both classes along track 164 of Jason-3 were nearly equal (~50%). The high percentage of non-Brown class in this area was mainly due to the existence of North Maluku mainland and small islands (e.g., Ju Island, Gebe Island, Sajang Island, Gag Island, Boo Island, Obira Island, and Gumumu Island). These influenced and contamina-ted the waveforms, thus creating the non-Brown pattern. Since the area had a steep contour topography (Figure 2), non-Brown waveforms were still found at deep water (>200 m). For instance, over Jason-3 pass 253, non-Brown waveforms were found at waters depth of 1071 m with a distance of 7.2 km from the land.

Waveforms in different water depth and distances to coastline (Figure 2 and Table 2) had different shapes due to varying combination of both land and sea bottom topography. These produced different noise levels in the waveform. Previous results in the Java Sea [25] showed that the higher the complexity of coastline topography, the more complicated the waveform shapes. [22] also reported that altimetry waveform depends on the distance between the altimeter footprint and the coastline, the type of the coastal terrains, and the shape of shorelines.
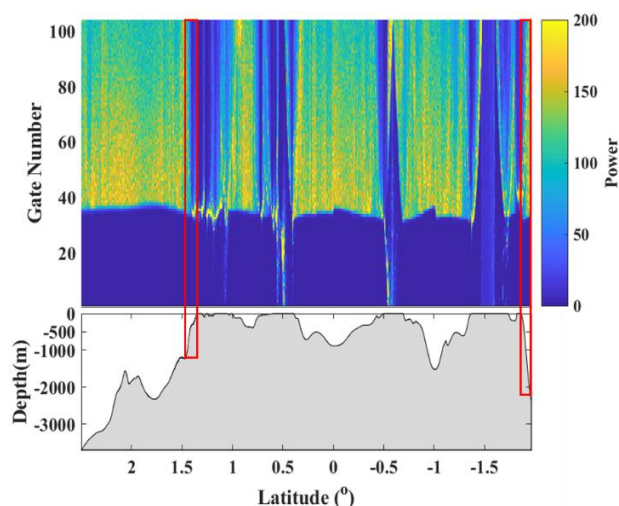
Figure 2 Echogram of Jason-3 pass 253 waveforms in the Halmahera Sea (top). The associated latitude (in degree) and depth (in m) are also shown (bottom). Red box indicates the non-Brown waveform at the steep contour waters

When the waveforms were further analyzed visually (or manually), the results showed that the waveforms over the Halmahera Sea have ten generic classes (Figure 3). Table 2 summarizes the waveform classes with their characteristics, distance to coastline, water depth, the coastal topography and percentage.

Off the ten classes, eight classes (Class 1-8) were the non-Brown waveform and two classes (Class 9-10) were the Brown. In general, classes 1-4 tend to be peaky patterns, either single peak or multi peak (Figure 3(a-d)), because they have a great influence from the land and sea bottom. They were found in near bay and small islands that had shallow waters (<200 m) and were close to the coastline (<17 km). Several studies in other regions reported similar findings, in which the peaky waveforms were found near to the coastline [8, 25, 29, 46, 47]. [8] also found that the highest percentage of peaky waveform was onshore, 5-6 km from the coastline.

Classes 5-8 (Figure 3(e-h)) were the waveforms with disturbed trailing edge. They generally had either additional peaks (with increased power) or strong decreased power at the trailing edge. These classes were mostly found at deep water (>200 m) and were close to the coastline (up to 86 km). The classes correspond to waveforms with a hyperbolic (class 5 and 6), a rise (class 7), and a fall (class 8) trailing edge. [8, 48] reported that the changes in the trailing edge could be defined by the changes in sea state in the littoral band. It indicated mostly reflection on specular surfaces in regions of weak winds and weak waves (sigma0 bloom events). The other factors, such as surface slicks, rain cells and cloud effects could also lead to the trailing edge changes [48].

Table 2 Generic classes in Halmahera Sea

Generic Class	Class characteristics	Distance to coastline (km)	Depth (m)	Coastal topography	Percentage (%)
Class 1	Quasi-specular shape	0.3 - 4.7	1 - 307	Bay and small strait	1.1
Class 2	Peaky with noise on decreasing part	0.3 - 16.6	2 - 200	Bay and small islands waters	2.3
Class 3	Peaky with noise on leading edge	0.3 - 5.8	2 -149	Bay and small islands waters	0.1
Class 4	Peaky with noise on leading edge and decreasing part	0.3 - 8.6	5 - 522	Bay and waters near to mainland	2.8
Class 5	Brown with noise echoes on trailing edge	0.6 – 86	19 - 3100	Wide bay and small islands waters	6.7
Class 6	Brown with peak on trailing edge	0.3 - 11.4	1 - 2377	Bay, strait, and small islands waters	4.9
Class 7	Brown with increasing trailing edge	2.8 - 12.2	114 - 840	Bay and small islands waters	1.0
Class 8	Brown with strong decreasing plateau	0.3 - 21.4	17 - 2377	Bay and strait	0.7
Class 9	Brown with shifted midpoint of leading edge	1.1 - 128.5	38 - 4367	Bay, small islands waters, waters near mainland, and offshore	62.9
Class 10	Ideal Brown	4.4 - 137.6	4 - 3034	Offshore	17.6
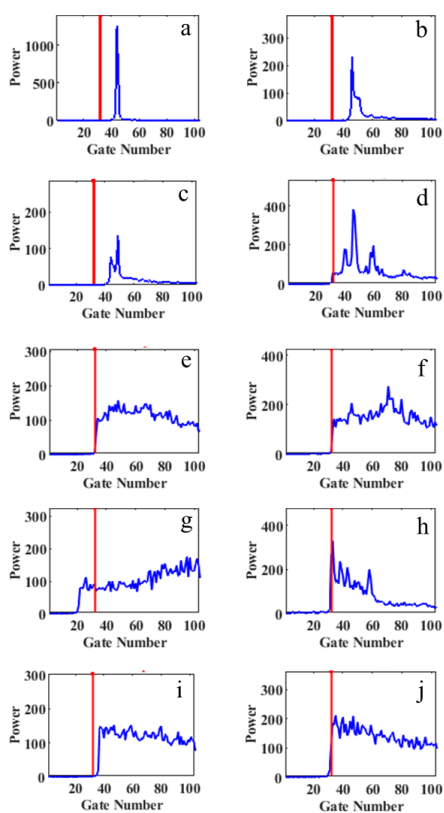
Figure 3 The Jason-2 and Jason-3 waveform classes in the Halmahera Sea (the red line is the tracking gate). (a) Class 1, (b) Class 2, (c) Class 3, (d) Class 4, (e) Class 5, (f) Class 6, (g) Class 7, (h) Class 8, (i) Class 9, (j) Class10

In general, the deeper and farther the waters from the land, the waveform pattern received by the satellite altimeter was getting closer to the ideal Brown pattern (class 10). However, due to the variability of sea states (e.g. surface roughness, wave, and rain), Brown waveforms with shifted mid-point of leading edge (class 9) might be observed. Class 9 and 10 could be found both onshore and offshore up to 138 km.

The finding in Table 2 showed that the ideal Brown waveform has a small percentage. Instead, the dominant class in the Halmahera Sea was class 9 (Figure 3i). In addition, the percentage of classes 1-8 is also quite high (>15 %) that are non-Brown. This indicated that more than 50% of the estimated SSHs in the Halmahera Sea was suspected to be inaccurate. The finding from this section alerted the need of waveform retracking to optimize the estimation of SSHs.

4.2   Evaluation of Waveform Retracking Performance against Geoid Height

The results of waveform retracking showed that each retracker had different performance, both spatially and temporally. Waveform retracking results on the same track but different periods gave different performances. For example, temporal retracking result of Jason-3 pass 164 showed that all retrackers applied in Halmahera Sea produced a low IMP in November 2016 (<20%), produced varying IMPs (ranging from 3% to 73%) in May 2017, and equally produced a high IMP in September 2017 (> 45%). Waveform retracking results on different tracks also gave different performances. The performance difference was due to the power and shape difference of the waveform, which was affected by the water surface roughness at different times or seasons. [28] reported that the retracking results in the shallow and narrow bay waters were better compared to the deep and wide bay waters and small islands waters.

other retrackers described only <70%. It was also seen that the mean correlation of Th 20% and ITh 20% were similar for those four distance bands, suggesting that their performances were equal.

Table 5 Mean of correlation at any distance from land. The best mean of correlations are shown in bold

Retracker	Mean of Correlation			
	0 - 5 km	5 - 10 km	10 - 15 km	15 - 20 km
OCOG	0.17	0.31	0.42	0.47
Th 10%	0.69	0.75	0.77	0.78
Th 20%	**0.71**	0.78	0.80	**0.79**
Th 50%	0.51	0.78	0.81	0.76
ITh 10%	0.69	0.76	0.78	0.78
ITh 20%	**0.71**	0.78	0.80	**0.79**
ITh 50%	0.50	0.78	**0.82**	0.76
Ice	**0.71**	**0.79**	0.81	**0.79**

Th is Threshold and ITh is Improved Threshold

Similar findings were reported by [27] where the performance of Ice retracker was found excellent within 0-5 km over the Ko Taphao Noi tide gauge in Thailand. It showed the average correlation of 0.78 [27]. This was presumably because the Gebe tide gauge station and Taphao Noi station were in the same waters condition (small islands waters).

Table 6 Mean of RMSE at several distance bands from coastline

| Retracker	Mean of RMSE (cm)			
	0 - 5 km	5 - 10 km	10 - 15 km	15 - 20 km
OCOG	156	105	48	63
Th 10%	24	22	23	23
Th 20%	**23**	21	21	**22**
Th 50%	37	**20**	**20**	27
ITh 10%	24	22	22	23
ITh 20%	**23**	21	21	**22**
ITh 50%	40	**20**	**20**	26
Ice	**23**	**20**	**20**	23

Th is Threshold and ITh is Improved Threshold

The SLAs correlation of Ice and Improved Threshold algorithm at Gebe station within of 0 – 5 km from the land was higher than the retracking result on the Croatian coast and the Italian coast by [16]. The results of the SLAs correlation of the Ice and Improved Threshold algorithm on the Croatian coast reached only 0.5 at a distance of 3 km from the land and 0.2 on the Italian coast within 4-5 km from the land [16]. The difference was due to the water condition difference of the tide gauge stations, which affect the shape of

the waveform and produce different SLAs estimates. It also attested the statement of [13] and [15] that the performance of each retracker differs depending on water conditions [13, 15].

The difference level in retracked SLAs to TG data in this study was shown by the value of Root Mean Square Error (RMSE). The results of waveform retracking in the Halmahera Sea showed a good mean RMSE (<30 cm) within 20 km from the land (Table 6). This result was similar to the results of the validation of the Ice algorithm conducted by Abdullah et al. (2017) in several areas of the TG station around the South China Sea within 30 km from the mainland [24].

Different results were found on the OCOG algorithm, which gives poor results on RMSE calculations. OCOG algorithm was only able to achieve the best mean RMSE at a distance of 10-15 km from the land (48 cm). These results were better than Ocean retracker results which had a lot of empty data within 0-20 km from the land (Figure 4), thus the mean of correlation and RMSE could not be calculated.
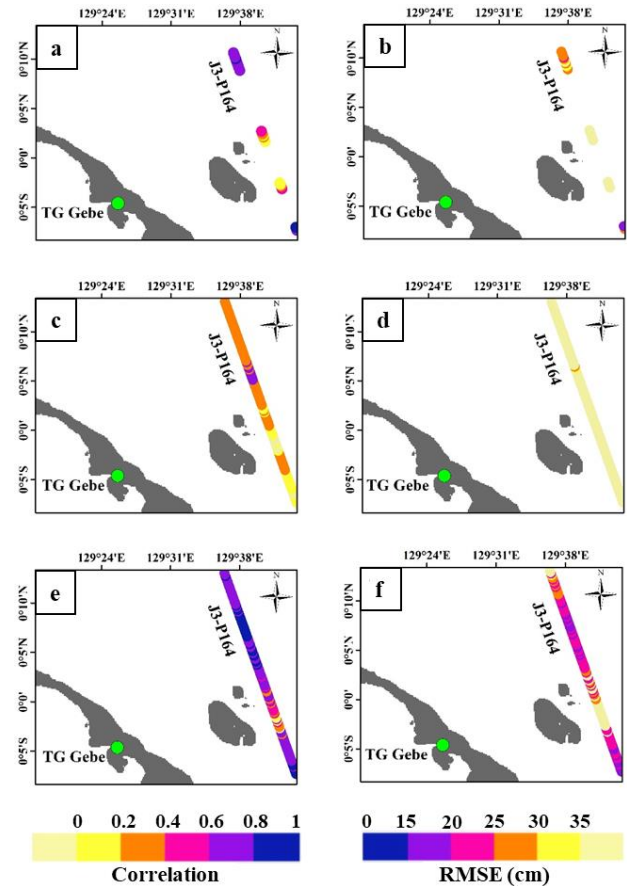
Figure 4 Spatial plot of temporal correlation and RMSE near Gebe tide gauge (TG Gebe) from retrackers: Ocean (a,b); OCOG (c, d); and Ice (e, f)

The spatial plot of temporal correlation and RMSE SLAs from Ocean retracker, OCOG, and Ice algorithm near TG Gebe station are shown in Figure 4. In general, the farther from the land, the higher the correlation and RMSE of those retrackers even though the Ocean retracker result had a vacancy data. This is indicated by the darker color at a distance further from the land, both in the correlation and RMSE figures. These results were consistent with the correlation and RMSE results obtained by Idris (2019) [27].
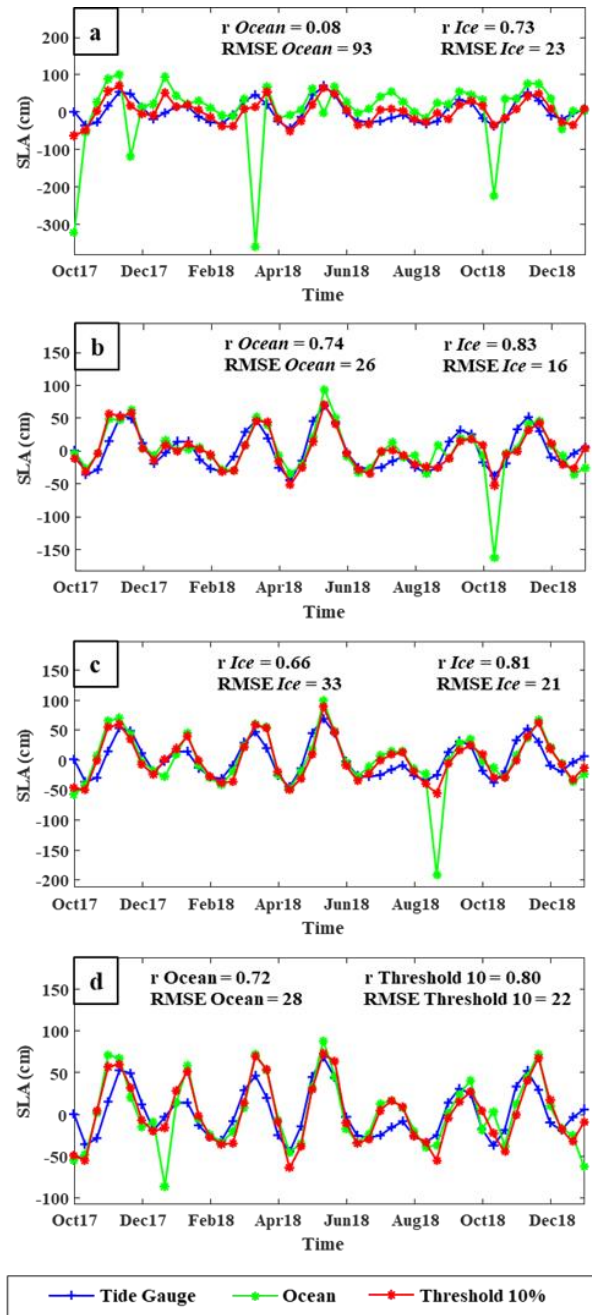
Figure 5 Time series of SLAs from different retrackers at different distance from the coastline. a) 5 km from the land, (b) 10 km from the land, (c) 15 km from the land, (d) 20 km from the land

SLAs produced by OCOG retrackers showed varying correlations within 0-20 km from the land even though they were dominated by correlations below 0.4 (Figure 4c). This variation was not apparent in the RMSE produced by OCOG, which mostly had RMSE above 35 cm (Figure 5d). This was in contrast to the results of the Ice retracker which had good correlation and RMSE results (Figure 4e and Figure 4f). The Ice retracker recorded the correlation between 0.6 and 1 and RMSE within15-25 cm.

The temporal SLAs of the Ocean retracker and the results of the Ice retracker at different distances are shown in Figure 5. The SLAs of Ice retracker appeared to have a pattern similar to the SLAs of TG Gebe at distances of 5 km, 10 km, 15 km and 20 km. This was supported by a high correlation value up to 0.86 and a low RMSE up to 16 cm at a distance of 10 km from the land. The results of Ice retracker were able to improve and provide better data than the standard Ocean algorithm at close distances to the land. Ocean SLAs had fluctuating pattern characterized by sharp valleys and produced a low correlation and a high RMSE to TG Gebe. The lowest results of the Ocean algorithm were located at a distance of 5 km from the land with a correlation of 0.08 and RMSE of 93 cm. In addition, within 10 km from the land invalid measurements were founds, which was nearly similar to the diameter of the Jason altimeter footprint (~7 km) [43].

In other different region, [49] reported better correlation and RMSE (up to 0.92 and 4.5 cm, respectively) between coastal altimetry product and tide gauge measurement over the Gulf of Genoa, Italy. This different result could be directly linked to local topography and environmental conditions, which have a strong influence on local sea level variability. Furthermore, differences in algorithms, corrections used, and the tide gauge distance to the altimetry track all had a significant impact on the result.

Based on the results from this study, the waveforms in the Halmahera Sea were very complex and vary depending on water conditions, so no one has as yet found the best retracker. In other words, the performance difference of each retracker in Halmahera Sea was generally not significant. Further research using a system that could classify waveform and automatically choose the appropriate retracker will provide the best SSHs in every water condition.

4.0 CONCLUSION

Waveforms of Jason-2 and Jason-3 in Halmahera waters had 10 dominant waveform classes that were influenced by the complexity of depth and distance from land. The waveforms in shallow water and near to the land were dominated by the peaky pattern while the waveforms in deep waters, but close to the land, had the perturbation trailing edge. Furthermore, waveforms in deep waters and far from land were dominated by Brown pattern. The highest waveform

percentage in Halmahera was the Brown waveform with shifted center point of leading edge.

The retracking results showed that all retrackers provided significant improvement in SSHs estimations except OCOG. The validation results also showed that all retrackers except OCOG had an average correlation above 0.75 and RMSE below 25 cm at a distance of 5-20 km from the land. However, the Threshold 10% was the most common retracker that appeared with the highest IMP, while Ice consistently produced the best correlation and RMSE the highest correlation of 0.86 and the lowest RMSE of 16 cm.

Acknowledgment

References

[1] Nababan, B., Hadiati, S. and Natih, N. M. N. 2015. Dynamic of Sea Level Anomaly of Indonesian Waters. *Jurnal Ilmu dan Teknologi Kelautan Tropis*. 7(1): 259-272.

[2] Handoko, E. Y. , Fernandes, M. J. and Lázaro, C. 2017. Assessment of Altimetric Range and Geophysical Corrections and Mean Sea Surface Models-Impacts on Sea Level Variability Around The Indonesian Seas. Remote Sensing.
DOI: http://dx.doi.org/10.3390/rs9020102.

[3] Lumban-gaol, J., Tambunan, E. and Osawa, T. 2017. Sea Level Rise Impact on Eastern Coast of North Sumatra, Indonesia. *2nd Int Forum Sustain Futur Asia, 2nd NIES Int Forum.*

[4] Chelton, D. B., Ries, J. C., Haines, B. J., Fu, L., and Callahan, P. 2001. *Satellite Altimetry. In A Handbook of Techniques and Applications.* San Diego (US): Academic Press. 1-132.

[5] Dumont, J. P., Romurduc, V., Carrere, L., Picot, N., Bronner, E., Couhert, A., Desai, S., Bonekamp, H., Scharroo, R., & Leuliette, E. 2017. OSTM/Jason-2 Products Handbook. 1-67.

[6] Dumont, J. P., Romurduc, V., Carrere, L., Picot, N., Bronner, E., Couhert, A., Guillot, A., Desai, S., & Bonekamp, H. 2017. Jason-3 Products Handbook. 1-62.

[7] Quartly, G. D., Srokosz, M. A. and McMillan, A. C. 2001. Analyzing Altimeter Artifacts: Statistical Properties of Ocean Waveforms. *Journal of Atmospheric Ocean Technology.* 18(12): 2074-2091.
DOI:http://dx.doi.org/10.1175/15200426(2001)018<2074:AA ASPO>2.0.CO;2.

[8] Gommenginger, C., Thibaut, P., Fenoglio-Marc, L., Quartly, G., Deng, X., Gomez-Enri, J., Challenor, P., & Gao, Y. G. 2011. *Retracking Altimeter Waveforms Near The Coasts. In Coastal Altimetry.* Berlin: Springer. 61-101.

[9] Brown, G. S. The Average Impulse Response of a Rough Surface and Its Applications. 1977. *IEEE Journal of Oceanic Engineering.* 2(1): 67-74.
DOI: http://dx.doi.org/10.1109/JOE.1977.1145328.

[10] Deng, X., and Featherstone, W. E. 2006. A Coastal Retracking System for Satellite Radar Altimeter Waveforms: Application to ERS-2 Around Australia. 2006. *Journal of Geophysical Research: Ocean.* 111(6): 1-16.
DOI: http://dx.doi.org/10.1029/2005JC003039

[11] Bao, L., Lu, Y. and Wang, Y. 2009. Improved Retracking Algorithm for Oceanic Altimeter Waveforms. *Progress in Natural Science.* 19(2): 195-203.
DOI: http://dx.doi.org/10.1016/j.pnsc.2008.06.017.

[12] Hwang, C., Guo, J., Deng, X., Hsu, H. Y., & Liu, Y. 2006. Coastal Gravity Anomalies from Retracked Geosat/GM Altimetry: Improvement, Limitation and The Role of Airborne Gravity Data. *Journal of Geodesy.* 80(4): 204-16.
DOI: http://dx.doi.org/10.1007/s00190-006-0052-x.

[13] Yang, L., Lin, M., Bai, Y., and Pan, D. 2008. Retracking Jason-1 Altimeter Waveform over China Coastal Zone. In *Microwave Remote Sensing of the Atmosphere and Environment VI.*
DOI: 10.1117/12.804835.

[14] Lee, H., Shum, C. K., Emery, W., Calmant, S., Deng, X., Kuo, C. Y., Roesler, C., & Yi, Y. 2010. Validation of Jason-2 Altimeter Data by Waveform Retracking over California Coastal Ocean. *Marine Geodesy.* 33(S1): 304-316.
DOI: http://dx.doi.org/10.1080/01490419.2010.488982.

[15] Guo, J. Y., Gao, Y. G., Chang, X. T., & Hwang, C. 2010. Optimized Threshold Algorithm of Envisat Waveform Retracking over Coastal Sea. Chinese *Jounal of Geophysics.* 53(4): 610-616.
DOI: http://dx.doi.org/10.1002/cjg2.1490.

[16] Roscher, R., Uebbing, B. and Kusche, J. 2017. STAR: Spatio-Temporal Altimeter Waveform Retracking Using Sparse Representation and Conditional Random Fields. *Remote Sensing of Environment.* 201: 148-164.
DOI: http://dx.doi.org/10.1016/j.rse.2017.07.024.

[17] Guo, J. Y., Gao, Y. G., Hwang, C. W., & Sun, J. L. 2010. A Multi-subwaveform Parametric Retracker of The Radar Satellite Altimetric Waveform and Recovery of Gravity Anomalies over Coastal Oceans. *Science China Earth Sciences.* 53(4): 610-616.
DOI: http://dx.doi.org/10.1007/s11430-009-0171-3.

[18] Sandwell, D. T., and Smith, W. H. F. 1997. Marine Gravity Anomaly from Geosat and ERS-1 Satellite Altimetry. *Journal of Geophysical Research: Solid Earth.* 163: 79-89
DOI: http://dx.doi.org/10.1029/96JB03223.

[19] Idris, N. H., and Deng, X. The Retracking Technique on Multi-Peak and Quasi-Specular Waveforms for Jason-1 and Jason-2 Missions near the Coast. 2012. *Marine Geodesy.* 35(S1): 217-237.
DOI: http://dx.doi.org/10.1080/01490419.2012.718679.

[20] Passaro, M., Cipollini, P., Vignudelli, S., Quartly, G. D., & Snaith, H. M. 2014. ALES: A Multi-mission Adaptive Subwaveform Retracker for Coastal and Open Ocean Altimetry. *Remote Sensing of Environment.* 145: 173-189.
DOI: http://dx.doi.org/10.1016/j.rse.2014.02.008.

[21] Idris, N. H., Deng, X., Din, A. M. M., and Idris, N. H. 2017. CAWRES: A Waveform Retracking Fuzzy Expert System for Optimizing Coastal Sea Levels from Jason-1 and Jason-2 Satellite Altimetry Data. *Remote Sensing.* 9(603): 1-22.
DOI: http://dx.doi.org/10.3390/rs9060603.

[22] Yang, L., Lin, M., Liu, Q., and Pan, D. A. 2012. Coastal Altimetry Retracking Strategy Based on Waveform Classification and Sub-Waveform Extraction. *International Journal of Remote Sensing.* 33(24): 7806-7819.
DOI: http://dx.doi.org/10.1080/01431161.2012.701350.

[23] Hakim, M. R., Nababan, B. and Panjaitan, J. P. 2015. Accuracy Improvement on Sea Surface Height Estimation Based on Waveform Retracking Analyses of Jason-2 Satellite in Java Sea. *Jurnal Ilmu dan Teknologi Kelautan Tropis.* 7(2): 771-790.
DOI: http://doi.org/10.29244/jitkt.v7i2.11254.

[24] Abdullah, N. N., Idris, N. H., Idris, N. H., Rahman, M. Z. A., &

Kadir, W. H. W. Regional Validation of Retracked Sea Levels from SARAL/Altika over The South China Sea and Adjacent Seas. *ARPN J Eng Appl Sci.* 12(23): 6622-6632.

[25] Nababan, B., Hakim, M. R. and Panjaitan, J. P. 2018. Waveform Identification and Retracking Analyses of Jason-2 Altimeter Satellite Data for Improving Sea Surface Height Estimation in Southern Java Island Waters and Java Sea, Indonesia. In *IOP Conference Series: Earth and Environmental Science.* 149: 1-13.
DOI: http://dx.doi.org/10.1088/1755-1315/149/1/012057.

[26] Wang, X., Ichikawa, K. and Wei, D. 2019. Coastal Waveform Retracking in Slick-Rich Sulawesi Sea of Indonesia, Based on Variable Footprint Size with homogeneous Sea Surface Roughness. *Remote Sensing.* 11(1274): 1-17.
DOI: http://dx.doi.org/10.3390/rs11111274.

[27] Idris, N. H. 2019. Regional Validation of The Coastal Altimetry Waveform Retracking Expert System (CAWRES) over The Largest Archipelago in Southeast Asian Seas. *International Journal of Remote Sensing.* 00(00): 1-15.
DOI: http://dx.doi.org/10.1080/01431161.2019.1681605.

[28] Sinurat, M. E. B., Nababan, B. and Lumban-Gaol, J. 2019. Waveform Retracking Analyses of Altimetry Satellite Data around Gulf, Small Islands, and Deep Waters in Halmahera Sea. *Jurnal Ilmu dan Teknologi Kelautatan Tropis.* 11(3): 793-807.
DOI: http://doi.org/10.29244/jitkt.v11i1.27101.

[29] Permana, R. D., Nababan, B. and Panjaitan, J. P. 2020. Waveform Re-tracking Analyses with Fuzzy Logic on Altimetry Satellite Data in Natuna Sea. In *IOP Conference Series: Earth and Environmental Science.* 429: 1-14.
DOI: http://dx.doi.org/ 10.1088/1755-1315/429/1/012042.

[30] Cortes, C., and Vapnik, V. 1995. Support-Vector Networks. *Machine Learning.* 20: 273-297.
DOI: http://dx.doi.org/10.1023/A:1022627411411.

[31] Beleites, C., Bonifacio, A., Codrich, D., Krafft, C., and Sergo, V. 2013. Raman Spectroscopy and Imaging: Promising Optical Diagnostic Tools in Pediatrics. *Current Medicinal Chemistry.* 760: 25-53.
DOI: http://dx.doi.org/10.2174/0929867311320170003.

[32] Amarouche, L., Thibaut, P., Zanife, O. Z., Dumont, J. P., Vincent, P., and Steunou, N. 2004. Improving the Jason-1 Ground Retracking to Better Account for Attitude Effects. *Marine Geodesy.* 27: 171-197.
DOI: http://dx.doi.org/10.1080/01490410490465210.

[33] Bamber, J. L. 1994. Ice Sheet Altimeter Processing Scheme. *International Journal of Remote Sensing.* 15(4): 925-938.
DOI: http://dx.doi.org/10.1080/01431169408954125.

[34] Wingham, D. J., Rapley, C. G. and Griffiths, H. 1986. New Techniques in Satellite Altimeter Tracking Systems. *Proceedings IGARSS'86 Symposium Diges.* 1: 185-190.

[35] Davis, C. H. 1995. Growth of The Greenland Ice Sheet: A Performance Assessment of Altimeter Retracking Algorithms. *IEEE Transactions on Geoscience and Remote Sensing.* 33(5): 1108-1116.
DOI: http://dx.doi.org/10.1109/36.469474.

[36] Davis, C. H. 1997. A Robust Threshold Retracking Algorithm for Measuring Ice-Sheet Surface Elevation Change from Satellite Radar Altimeters. *IEEE Transaction on Geoscience and Remote Sensing.* 35(4): 974-979.
DOI: http://dx.doi.org/10.1109/36.602540

[37] Anzenhofer, M., Shum, C. K. and Rentsh, M. 1999. *Coastal Altimetry and Applications.* Ohio State University Geodesy.

[38] Yang, Y., Hwang, C., Hsu, H. J, Dongchen, E., & Wang, H. 2012. A Subwaveform Threshold Retracker for ERS-1 Altimetry: A Case Study in the Antarctic Ocean. *Computers & Geosciences.* 41: 88-98.
DOI: http://dx.doi.org/10.1016/j.cageo.2011.08.017.

[39] Andersen, O. B., and Scharroo, R. 2011. Range and Geophysical Corrections in Coastal Regions: and Implications for Mean Sea Surface Determination. In Coastal Altimetry. Berlin (DE): Springer. 103-145.
http://weekly.cnbnews.com/news/article.html?no=124000

[40] Labroue, S., Gaspar, P., Dorandeu, J., Zanife, F., Mertz, F., Vincent, P., and Choquet, D. 2004. Non Pparametric Estimates of The Sea State Bias for The Jason-1 Radar Altimeter. *Marine Geodesy.* 27(3-4): 453-481. DOI: 10.1080/01490410490902089.

[41] Pawlowicz, R., Beardsley, B., Lentz, S. 2002. Classical Tidal Harmonic Analysis Including Error Estimates in MATLAB Using T_TIDE. *Computer & Geosciences.* 28: 929-937.
DOI: https://doi.org/10.1016/S0098-3004(02)00013-4.

[42] Idris, N. H., Deng, X., and Andersen. O. A. 2014. The Importance of Coastal Altimetry Retracking and Detiding: A Case Study around the Great Barrier Reef, Australia. *International Journal of Remote Sensing.* 35(5): 1729-1740. Doi:10.1080/01431161.2014.882032.

[43] Vignudelli, S., Birol, F., Benveniste, J., Fu, L-L., Picot, N., Raynal, M., and Roinard, H. 2019. Satellite Altimetry Measurements of Sea Level in the Coastal Zone. *Survey in Geophysics.* 40: 1319-1349. DOI: 10.1007/s10712-019-09569-1.

[44] Emery, W. J., and Thomson, R. E. 2001. Time-series Analysis Methods. In Data Analysis Methods in Physical Oceanography.
DOI: http://dx.doi.org/10.1016/b978-044450756-3/50006-x.

[45] Idris, N. H., Vignudelli, S., Deng, X. 2020. Assessment of retracked sea levels from Sentinel-3A Synthetic Aperture Radar (SAR) Mode Altimetry over The Marginal Seas at Southeast Asia. *International Journal of Remote Sensing.* 42(4): 1535-1555. DOI: 10.1080/01431161.2020.1836427.

[46] Deng, X., Featherstone, W. E., Hwang, C., & Berry, P. A. M. 2002. Estimation of Contamination of ERS-2 and POSEIDON Satellite Radar Altimetry Close to the Coasts of Australia. *Marine Geodesy.* 25(4): 249-71.
DOI: http://dx.doi.org/10.1080/01490410214990.

[47] Lumban-Gaol, J., Adrian, D., Vignudelli, S., Leben, R. R., Nurjaya, I. W., Osawa, T., Manurung, P., & Arhatin, R. E. 2018. An Assessment of A Coastal Altimetry Data Product in The Indonesian Waters. In *IOP Conference Series: Earth and Environmental Science.* 176: 1-10.
DOI: 10.1088/1755-1315/176/1/012034.

[48] Thibaut, P., Poisson, J. C., Bronner, E., & Picot, N. 2010. Relative Performance of MLE3 and MLE4 Retracking Algorithms on Jason-2 Altimeter Waveforms. *Marine Geodesy.* 33(S1): 317-335.
DOI: 10.1080/01490419.2010.491033.

[49] Picco, P., Vignudelli, S., and Repitti, L. 2020. A Comparison between Coastal Altimetry Data and Tida; Gauge Measurements in the Gulf of Genoa (NW Mediterranean Sea). *Journal of Marine Science and Engineering.* 8(862):1-16. DOI: 10.3390/jmse8110862.